Near-field optical contrasts in the Fresnel evanescent wave

Christian Girard
CEMES/CNRS, 29 rue Jeanne-Marvig, Boîte Postale 4347, 31055 Toulouse Cedex 4, France

Alain Dereux and Jean-Claude Weeber
Laboratoire de Physique, Optique Submicronique, Université de Bourgogne, 21011 Dijon Cedex, France
(Received 17 February 1998)

The surface waves generated by total internal reflection at the surface of a transparent material may be viewed as quasi-two-dimensional, because they decay exponentially in the direction normal to the sample surface. These waves are appropriate to analyze polarization effects associated with light confinement phenomena in near-field optics. In this paper we derive four useful analytical relations governing the near-field contrast around dielectric nanometer-sized particles versus a limited number of external parameters. In the *p*-polarized mode, unlike to what happens with the electric near field, we show that the magnitude of the magnetic near-field contrast can be adjusted by increasing the incident angle beyond the critical angle. [S1063-651X(98)01407-X]

PACS number(s): 42.30.Yc, 33.80.−b, 78.66.−w, 85.40.Ux

I. INTRODUCTION

The physics of optical evanescent waves (OEW) which is the central concept used in near-field optics (NFO) instrumentation has been familiar in traditional optics for a long time. The analysis of the skin depth effect at metallic surfaces was probably the first recognition of the existence of evanescent electromagnetic waves [1,2]. In modern physics, the control of such peculiar light fields provides an interesting and versatile tool that generates powerful applications (tunneling time measurements [3], highly resolved microscopy and spectroscopy [4], atomic physics [5,6], etc.). For example, in *laser cooled atom* physics such phenomena can be used as adjustable ''atomic mirrors.'' Under certain conditions, it is even possible, by adjusting the force field associated with the OEW to balance the van der Waals forces between a small number of cooled atoms and the neighboring surface. The control of the different optical parameters (incident angle, polarization, wavelength, etc.) leads to new noninvasive atomic manipulation processes [5].

About ten years ago, in a different context, the attenuated total reflection that uses the perturbation of a surface evanescent wave to measure the dispersion relations of interface polaritons gave rise to a particular configuration of scanning near-field optical microscope called the ''scanning tunneling optical microscope'' (STOM) [alternatively called ''photon scanning tunneling microscope'' (PSTM)] [7,8]. This concept has been tested and investigated by numerous experimental and theoretical studies [9]. One of the most fascinating observations realized with this local probe technique was the real-space mapping of the interference pattern created by two contrapropagating OEW near a glass substrate [10]. Indeed, in spite of their evanescent character, two different OEW have the capability of interfering over the supporting surface. The observation of this intriguing optical phenomena was first reported by Meixner *et al.* in the STOM-PSTM configuration. In particular, the extremely regular periodic intensity pattern above the surface can be used as a calibration tool for NFO instruments.

Currently, this photonic local probe added a new dimension to the study of the optical properties of small particles lying on a surface. Simultaneously, several adequate numerical methods have been developed to understand the near-field optical interaction with mesoscopic and nanoscopic objects [4]. These simulations clearly evidenced the different roles played by both *electric* and *magnetic* fields in the near zone [11]. They indicated unambiguously that the individual structures lying on the surface distort the optical near-field intensities established by the self-consistent interaction between the surface roughness and the incident light. Particularly, it was demonstrated that when the lateral dimensions of tiny objects are significantly smaller than the incident wavelength, the interference pattern collapses and the optical electric near-field intensity distribution tends to be fairly well localized around the objects [11]. Under well-defined conditions on the incident field (polarization, wavelength) a highly localized electric near-field intensity occurs just above the subwavelength protrusions. Recently these considerations facilitated the interpretation of this peculiar NFO phenomenon. For example, a simple dielectric cube of cross section 100×100 (nm^2) was imaged with the dielectric tip of a STOM-PSTM with a bright contrast when the surface wave was *p* polarized and with a dark contrast when it was *s* polarized [12].

Actually, the analysis of the numerical outputs yielded by those accurate numerical schemes may be made easier by elaborating upon some analytical expressions in which the main experimental parameters (incident angle, optical index, polarization modes, etc.) occur explicitly. In this paper we derive four useful analytical relations governing the near-field contrast around dielectric nanometer-sized particles versus a limited number of external parameters. In particular, from analytical arguments it will be demonstrated that unlike what happens with the electric near field, in the *p*-polarized mode the magnitude of the magnetic near-field contrast can be adjusted by increasing the incident angle beyond the critical angle for total reflection.

II. POLARIZED FRESNEL EVANESCENT WAVE

In this basic illumination mode, the surface wave is generated by illuminating the surface from underneath by a

monochromatic plane wave of frequency ω_0, incident at an angle θ_0 larger than θ_{tot}. Throughout the paper we will consider a transparent medium of optical index n. Two different incident polarizations can be considered: s polarization, where the incident electric field is parallel to the surface-air interface, and p polarization, where it is in the plane of incidence.

The incident field at an observation point $\mathbf{r}=(x,y,z)=(\mathbf{l},z)$ above the surface becomes

$$\mathbf{E_0}(\mathbf{r},t)=\mathbf{E_0}(\mathbf{r})e^{-i\omega_0 t}=\mathbf{E_0}e^{i\mathbf{k}\cdot\mathbf{l}}e^{-Kz}e^{-i\omega_0 t}, \tag{1}$$

where

$$K=\frac{\omega_0}{c}(\sin^2\theta_0-\sin^2\theta_{\mathrm{tot}})^{1/2}=k_0(n^2\sin^2\theta_0-1)^{1/2} \tag{2}$$

and

$$\|\mathbf{k}\|=nk_0\sin\theta_0. \tag{3}$$

When, for example, the incident field is propagating along the OY axis, one obtains for s polarization:

$$\begin{aligned} E_{0x}(\mathbf{r})&=A_0T_s,\\ E_{0y}(\mathbf{r})&=E_{0z}(\mathbf{r})=0, \end{aligned} \tag{4}$$

and for p polarization:

$$\begin{aligned} E_{0x}(\mathbf{r})&=0,\\ E_{0y}(\mathbf{r})&=A_0T_p\delta_c,\\ E_{0z}(\mathbf{r})&=A_0T_p\delta_s, \end{aligned} \tag{5}$$

where

$$\begin{aligned} \delta_s&=\frac{\sin(\theta_0)}{\sin(\theta_{\mathrm{tot}})},\\ \delta_c&=\frac{iK}{k_0\sin(\theta_{\mathrm{tot}})}. \end{aligned} \tag{6}$$

In Eqs. (2) and (3), A_0 is proportional to $e^{i\mathbf{k}\cdot\mathbf{l}}e^{-Kz}$, and the factors T_s and T_p are the usual transmission coefficients for each polarization. From these relations [Eqs. (1), (4), and (5)], we can obtain the magnetic field $\mathbf{B}_0(\mathbf{r},t)$ of the surface wave

$$\mathbf{B}_0(\mathbf{r},t)=\frac{c}{i\omega_0}\nabla\times\mathbf{E}_0(\mathbf{r},t). \tag{7}$$

III. COUPLING WITH A SUBWAVELENGTH-SIZED DIELECTRIC SPHERE

To illustrate the coupling between a polarized fresnel evanescent wave (PFEW) and a small spherical object lying on the sample, we consider the model system described in Fig. 1. The geometrical parameters used in this calculation are reported in the corresponding figure caption. The substrate modifies the polarizability $\alpha_0(\omega)$ of the particle. We then have

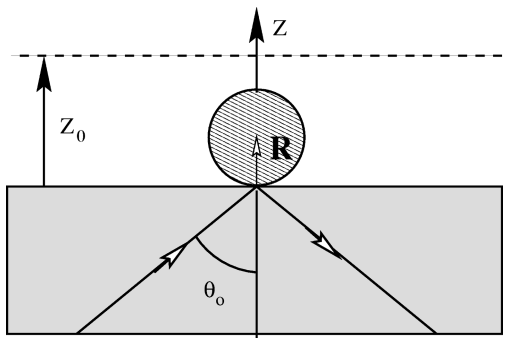

FIG. 1. Schematic drawing of the model system used in the present paper. A tranparent substrate, of optical index $n=1.5$, supports a small dielectric sphere of diameter D. The system is illuminated in total internal reflection with an incident angle θ_0 and $\mathbf{R}=(0,0,D/2)$.

$$\alpha^{ef}(\mathbf{R},\omega)=\alpha_0(\omega)\mathbf{M}(\mathbf{R},\omega) \tag{8}$$

with

$$\mathbf{M}(\mathbf{R},\omega)=[\mathbf{I}-\mathbf{S}(\mathbf{R},\mathbf{R},\omega)\alpha_0(\omega)]^{-1}, \tag{9}$$

where $\mathbf{S}(\mathbf{R},\mathbf{R},\omega)$ is the nonretarded propagator associated with the bare surface, and $\mathbf{R}=(0,0,R)$ labels the particle location. Within this description, the optical properties of the spherical particle-surface supersystem are described in terms of ''dressed'' polarizability. In the past, several theoretical works [13] have been devoted to its calculation with molecular systems interacting with simple substrates (spheres, cylinders, planes, etc.). If the particle polarizability $\alpha_0(\omega)$ is initially isotropic, the symmetry of the tensor $\alpha^{ef}(\mathbf{R},\omega)$ is governed mainly by the symmetry of the substrate. In the particular case of a single spherical particle interacting with a perfectly planar surface, the dyadic tensor $\mathbf{M}(\mathbf{R},\omega)$ becomes diagonal and, consequently, $\alpha^{ef}(\mathbf{R},\omega)$ belongs to the $C_{\infty v}$ symmetry group. In this case, α^{ef} may be described with two independent components $\alpha_{\|}^{ef}$ and $\alpha_{\perp}^{ef}$ [13–15]:

$$\alpha^{ef}(\mathbf{R},\omega)=\begin{pmatrix} \alpha_{\|}^{ef}(\mathbf{R},\omega) & 0 & 0\\ 0 & \alpha_{\|}^{ef}(\mathbf{R},\omega) & 0\\ 0 & 0 & \alpha_{\perp}^{ef}(\mathbf{R},\omega) \end{pmatrix} \tag{10}$$

with

$$\alpha_{\|}^{ef}(\mathbf{R},\omega)=\frac{8\alpha_0(\omega)R^3}{8R^3-\alpha_0(\omega)\Delta(\omega)} \tag{11}$$

and

$$\alpha_{\perp}^{ef}(\mathbf{R},\omega)=\frac{4\alpha_0(\omega)R^3}{4R^3-\alpha_0(\omega)\Delta(\omega)}. \tag{12}$$

In these two relations, the factor $\Delta(\omega)=[\epsilon(\omega)-1)]/[\epsilon(\omega)+1]$ is merely the nonretarded reflection coefficient of the surface. Let us notice that when working with two dielectric materials of low optical indexes, the anisotropic ratio defined by

TABLE I. Contrast in the *s* polarized mode.

Field intensity	θ_0 dependence	Sign of η	Predicted contrast	Decay law
Electric	negligible	negative	dark	r^{-3}
Magnetic	weak	positive	bright	r^{-2}

TABLE II. Same as in Table I but for the *p* polarized mode.

Field intensity	θ_0 dependence	Sign of η	Predicted contrast	Decay law
Electric	weak	positive	bright	r^{-3}
Magnetic	strong	negative	dark	r^{-2}

$$\xi=\frac{\alpha_{\perp}^{ef}}{\alpha_{\parallel}^{ef}} \tag{13}$$

remains always close to the unity over all the optical spectrum. In this case, we can easily verify that the effective polarizability of the particle can be replaced by the polarizability of the free particle with an excellent approximation. This approximation is no longer valid when dealing with metallic objects for which all further calculations must be performed on the basis of Eqs. (11) and (12).

IV. NEAR-FIELD CONTRASTS

A. Basic equations

At a point **r** located above the sample at the immediate proximity of the particle, the incident homogeneous surface wave is locally distorted. In fact, the fluctuating dipole moment $\mu(\mathbf{R},\omega_0)=\alpha^{ef}(\mathbf{R},\omega_0)\cdot\mathbf{E}_0(\mathbf{R},t)$ induced inside the particle, produces two additional contributions to the electromagnetic field. At the first Born approximation, we can write

$$\mathbf{E}(\mathbf{r},t)=\mathbf{E}_0(\mathbf{r},t)+\mathbf{S}_0(\mathbf{r},\mathbf{R})\cdot\alpha^{ef}(\mathbf{R},\omega_0)\cdot\mathbf{E}_0(\mathbf{R},t) \tag{14}$$

and

$$\mathbf{B}(\mathbf{r},t)=\mathbf{B}_0(\mathbf{r},t)+\mathbf{Q}_0(\mathbf{r},\mathbf{R},\omega_0)\cdot\alpha^{ef}(\mathbf{R},\omega_0)\cdot\mathbf{E}_0(\mathbf{R},t), \tag{15}$$

where the dyadic tensors $\mathbf{S}_0(\mathbf{r},\mathbf{R})$ and $\mathbf{Q}_0(\mathbf{r},\mathbf{R},\omega_0)$ are the two usual free space propagators that describe how an arbitrary dipole radiates electromagnetic energy [16]. In the near-field zone, i.e., when $|\mathbf{r}-\mathbf{R}|<\lambda_0=2\pi c/\omega_0$, they can be expressed by

$$\mathbf{S}_0(\mathbf{r},\mathbf{R})=\frac{3(\mathbf{r}-\mathbf{R})(\mathbf{r}-\mathbf{R})-|\mathbf{r}-\mathbf{R}|^2\mathbf{I}}{|\mathbf{r}-\mathbf{R}|^5} \tag{16}$$

and

$$\mathbf{Q}_0(\mathbf{r},\mathbf{R},\omega_0)=\frac{i\omega_0}{c|\mathbf{r}-\mathbf{R}|^3}\begin{pmatrix}0 & -(z-R) & y\\ z-R & 0 & -x\\ -y & x & 0\end{pmatrix}. \tag{17}$$

B. Dark or bright constrasts

Current experimental measurements provide us with many images in which the small surface protrusions generally appear with either dark or bright contrast, corresponding to either a smaller or a larger number of detected photons. In this section, from Eqs. (14) and (15), we will derive four useful analytical expressions that show explicitly the dependence of the near-field intensity constrast with respect to the external parameters. This can be achieved by defining two dimensionless coefficients depending on the location of the observation point **r**:

$$\eta_e(\mathbf{r})=\frac{|\mathbf{E}(\mathbf{r})|^2}{|\mathbf{E}_0(\mathbf{r})|^2}-1 \tag{18}$$

and

$$\eta_m(\mathbf{r})=\frac{|\mathbf{B}(\mathbf{r})|^2}{|\mathbf{B}_0(\mathbf{r})|^2}-1. \tag{19}$$

When the observation point (that could be physically materialized by a sharp probe) is located just on the top of the particle [i.e., when $\mathbf{r}=\mathbf{R}_0=(0,0,Z_0)$], both the sign and magnitude of these coefficients provide direct information on the light confinement phenomenon. Considering the two usual polarization modes (labeled by the subscripts *s* and *p*), we can then derive four formula.

(1) *s-polarized mode:*

$$\eta_{e,s}=-\frac{2\alpha_{\parallel}}{(Z_0-R)^3}\{1+o(|Z_0-R|^{-6})\} \tag{20}$$

and

$$\eta_{m,s}=\frac{2\alpha_{\parallel}k_0(n^2\sin^2\theta_0-1)^{1/2}}{(2n^2\sin^2\theta_0-1)(Z_0-R)^2}\{1+o(|Z_0-R|^{-4})\}. \tag{21}$$

(2) *p-polarized mode:*

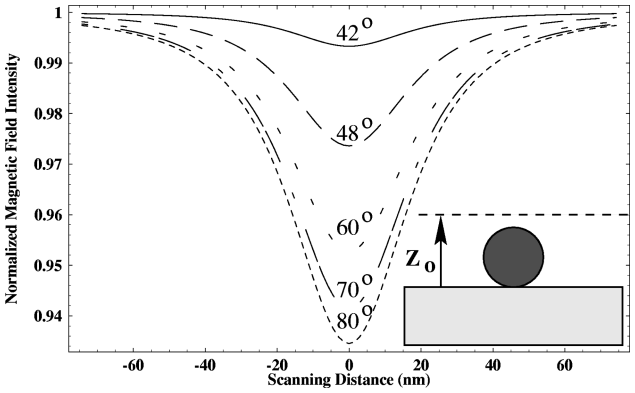

FIG. 2. Series of scanlines calculated above the topographic object described in Fig. 1 ($D=30$ nm). Five increasing values of θ_0 have been successively considered (42°, 48°, 60°, 70°, and 80°).

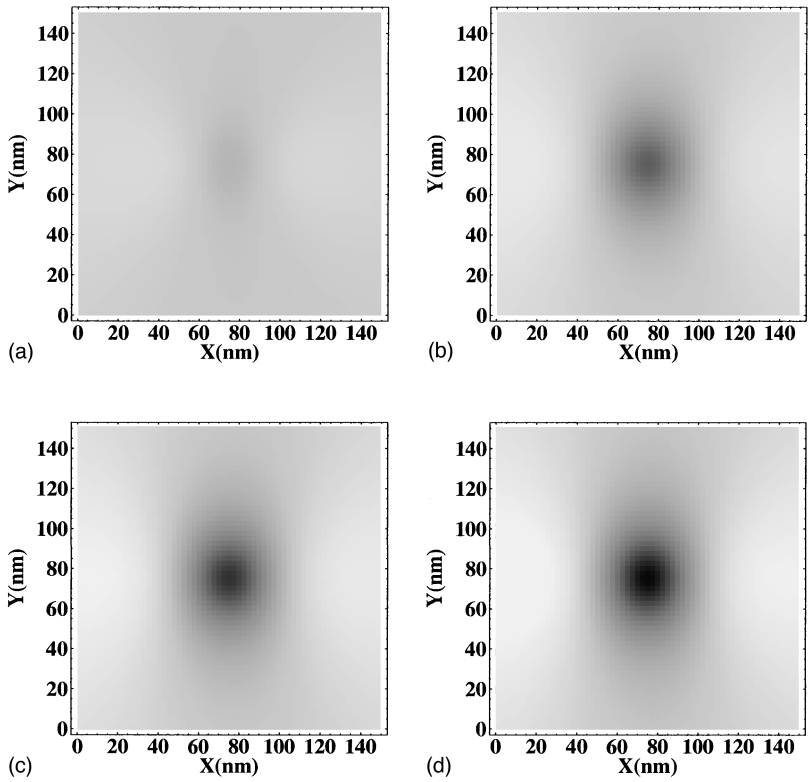

FIG. 3. Sequence of four images describing the evolution of the depression created in the magnetic intensity map above the same object (cf. Fig. 1) when increasing the incident angle: (a) $\theta_0=42°$, (b) $\theta_0=55°$, (c) $\theta_0=65°$, and (d) $\theta_0=80°$.

$$\eta_{e,p}=\frac{2\alpha_{\perp}(n^2\sin^2\theta_0+1)}{(n^2\sin^2\theta_0-1)(Z_0-R)^3}\{1+o(|Z_0-R|^{-6})\} \tag{22}$$

and

$$\eta_{m,p}=-\frac{2\alpha_{\perp}k_0(n^2\sin^2\theta_0-1)^{1/2}}{(Z_0-R)^2}\{1+o(|Z_0-R|^{-4})\}. \tag{23}$$

These simple relations can be used to analyze both the electric and magnetic contrasts near subwavelength dielectric particles. The main physical behaviors predicted by these relations are summarized in Tables I and II. Some comments can be made about these results.

(i) The more impressive success provided by these simple relations concerns the contrast. Indeed, when dealing with subwavelength-sized localized objects, the contrast predicted by the simple dipolar model is found in excellent agreement with available experimental data on similar objects [17,12,18]. Additionally, all physical behaviors gathered in Tables I and II are in agreement with the outputs produced by sophisticated *ab initio* Maxwell's equation solvers [11].

(ii) In the *p*-polarized mode, Eq. (23) predicts subwavelength-sized magnetic field intensity patterns with a strong and dark contrast that dramatically depends on the incident illumination angle θ_0. This phenomena is illustrated in Figs. 2 and 3 in which we have calculated the ratio variation

$$I_B(\mathbf{r})=\frac{|\mathbf{B}(\mathbf{r})|^2}{|\mathbf{B}_0(\mathbf{r})|^2} \tag{24}$$

upon scanning the observation point $\mathbf{r}$ in the plane $(X0Y)$ located at $Z_0=40$ nm above a dielectric sphere of diameter $D=30$ nm and optical index $n_{\mathrm{sph}}=1.5$. In this case, the magnetic contrast vanishes drastically when θ_0 gets closer and closer to the critical angle. For incident angles much larger than the critical angle, we observed a significant depression of the magnetic field intensity very well localized around the sphere. Although the complete angular investigation of this peculiar effect has not been yet realized, these trends seem to be in qualitative agreement with recent local measurement performed with metallic coated tips [18].

V. CONCLUSION

The elaboration of analytical models to support the ongoing development of the NFO (theory and instrumentation) can be viewed as a useful complementary tool of the numerous more sophisticated *ab initio* approaches [9]. Within the limit of the applicability range of such models (multipolar response theory, nonretarded limit, etc.) it is possible to bring to the fore the main intrinsic physical mechanisms responsible for the image formation in the near-field zone. In the near future, we plan to extend these analytical considerations to get more insight into the image formation processes in the presence of small metallic aggregates.

ACKNOWLEDGMENTS

The CEMES is LPR CNRS 8011. The Laboratoire de Physique is supported by the CNRS, and also benefits from the financial support of the Region of Burgundy.

[1] J. Zenneck, Ann. Phys. (Leipzig) **23**, 846 (1907).
[2] A. Sommerfeld, Ann. Phys. (Leipzig) **28**, 665 (1909).
[3] Ph. Balcou and L. Dutriaux, Phys. Rev. Lett. **78**, 851 (1997).
[4] *Near Field Optics*, Vol. 242 of *NATO Advanced Studies Institute Ser. E: Applied Sciences*, edited by D. W. Pohl and D. Courjon (Kluwer, Dordrecht, 1993) and references therein.
[5] A. Landragin, J.-Y. Courtois, G. Labeyrie, N. Vansteenkiste, C. I. Westbrook, and A. Aspect, Phys. Rev. Lett. **77**, 1464 (1996).
[6] T. Esslinger, M. Weidemüller, A. Hemmerich, and T. W. Hänsch, Opt. Lett. **18**, 450 (1993).
[7] R. C. Reddick, R. J. Warmack, and T. L. Ferrell, Phys. Rev. B **39**, 767 (1989).
[8] D. Courjon, K. Sarayedine, and M. Spajer, Opt. Commun. **71**, 23 (1989).
[9] C. Girard and A. Dereux, Rep. Prog. Phys. **59**, 657 (1996).
[10] A. Meixner, M. Bopp, and G. Tarrach, Appl. Opt. **33**, 7995 (1994).
[11] Ch. Girard, J.-C. Weeber, A. Dereux, O. J. F. Martin, and J.-P. Goudonnet, Phys. Rev. B **55**, 16 487 (1997).
[12] J. C. Weeber, E. Bourillot, A. Dereux, Y. Chen, J.-P. Goudonnet, and Ch. Girard, Phys. Rev. Lett. **77**, 5332 (1996).
[13] S. Efrima and H. Metiu, J. Chem. Phys. **70**, 1939 (1979).
[14] Ch. Girard, Pure Appl. Opt. **1**, 157 (1992).
[15] O. Keller, Phys. Rep. **268**, 85 (1996), and references therein.
[16] L. Landau and E. Lifshitz, *Théorie des Champs*, Tome II, Éditions (MIR, Moscow, 1970), pp. 256.
[17] D. Courjon (unpublished).
[18] J.-C. Weeber, Ph.D. thesis, University of Burgundy, Dijon, France (1996).